Journal of Structural Biology 213 (2021) 107674

Contents lists available at ScienceDirect

Journal of Structural Biology

journal homepage: www.elsevier.com/locate/yjsbi

Structure and substrate specificity determinants of the taurine biosynthetic enzyme cysteine sulphinic acid decarboxylase

Elaheh Mahootchi [a,1], Arne Raasakka [a,1], Weisha Luan [b], Gopinath Muruganandam [c,d], Remy Loris [c,d], Jan Haavik [a,e,*], Petri Kursula [a,b,f,*]

[a] Department of Biomedicine, University of Bergen, Bergen, Norway
[b] Faculty of Biochemistry and Molecular Medicine, University of Oulu, Oulu, Finland
[c] VIB-VUB Center for Structural Biology, Vlaams Instituut voor Biotechnologie, Brussels, Belgium
[d] Structural Biology Brussels, Department of Bioengineering Sciences, Vrije Universiteit Brussel, Brussels, Belgium
[e] Bergen Center of Brain Plasticity, Division of Psychiatry, Haukeland University Hospital, Bergen, Norway
[f] Biocenter Oulu, University of Oulu, Oulu, Finland

ARTICLE INFO

Keywords:
Cysteine sulphinic acid
Enzyme structure
Reaction mechanism
Substrate specificity
Pyridoxal phosphate

ABSTRACT

Pyridoxal 5́-phosphate (PLP) is an important cofactor for amino acid decarboxylases with many biological functions, including the synthesis of signalling molecules, such as serotonin, dopamine, histamine, γ-aminobutyric acid, and taurine. Taurine is an abundant amino acid with multiple physiological functions, including osmoregulation, pH regulation, antioxidative protection, and neuromodulation. In mammalian tissues, taurine is mainly produced by decarboxylation of cysteine sulphinic acid to hypotaurine, catalysed by the PLP-dependent cysteine sulphinic acid decarboxylase (CSAD), followed by oxidation of the product to taurine. We determined the crystal structure of mouse CSAD and compared it to other PLP-dependent decarboxylases in order to identify determinants of substrate specificity and catalytic activity. Recognition of the substrate involves distinct side chains forming the substrate-binding cavity. In addition, the backbone conformation of a buried active-site loop appears to be a critical determinant for substrate side chain binding in PLP-dependent decarboxylases. Phe94 was predicted to affect substrate specificity, and its mutation to serine altered both the catalytic properties of CSAD and its stability. Using small-angle X-ray scattering, we further showed that CSAD presents open/close motions in solution. The structure of apo-CSAD indicates that the active site gets more ordered upon internal aldimine formation. Taken together, the results highlight details of substrate recognition in PLP-dependent decarboxylases and provide starting points for structure-based inhibitor design with the aim of affecting the biosynthesis of taurine and other abundant amino acid metabolites.

1. Introduction

Pyridoxal 5-phosphate (PLP), the active form of vitamin B6, is a ubiquitous cofactor essential for a number of enzymes. PLP-dependent enzymes, which mainly use PLP as a covalently bound coenzyme, account for 4% of total cellular enzymatic activity (Percudani and Peracchi, 2003; Thornton et al., 2000). Mammalian genomes encode several PLP-dependent enzymes, which catalyse a variety of biochemical reactions using different substrates (Percudani and Peracchi, 2003; Liang et al., 2019). Many PLP-dependent enzymes use amino acids as substrates and play central roles in cellular metabolism.

PLP-dependent enzymes are established drug targets in cancer and neurological diseases. Inhibitors of γ-aminobutyric acid (GABA) aminotransferase are of therapeutic interest in central nervous system disorders, being used in the treatment of epilepsy (Sarup et al., 2003), and inhibitors of L-DOPA decarboxylase (DDC) are used in treating

Abbreviations: CA, cysteic acid; CD, circular dichroism; CSA, cysteine sulphinic acid; CSAD, cysteine sulphinic acid decarboxylase; DDC, L-DOPA decarboxylase; DSF, differential scanning fluorimetry; GABA, γ-aminobutyric acid; GAD, Glu decarboxylase; GADL1, GAD-like protein 1; HDC, histidine decarboxylase; MALS, multi-angle static light scattering; PLP, pyridoxal 5'-phosphate; PLP-DC, PLP-dependent decarboxylase; SAXS, small-angle X-ray scattering; SEC, size-exclusion chromatography; WT, wild-type.

* Corresponding authors at: Department of Biomedicine, University of Bergen, Bergen, Norway.
E-mail addresses: jan.haavik@uib.no (J. Haavik), petri.kursula@uib.no (P. Kursula).

[1] Equal contribution.

https://doi.org/10.1016/j.jsb.2020.107674
Received 3 October 2020; Received in revised form 13 November 2020; Accepted 21 November 2020
Available online 27 November 2020
1047-8477/© 2020 The Authors. Published by Elsevier Inc. This is an open access article under the CC BY license (http://creativecommons.org/licenses/by/4.0/).

Parkinson's disease (Bartholini and Pletscher, 1975; Sletzinger et al., 1963). Furthermore, recessive mutations in PLP-dependent enzymes are associated with severe neurological syndromes (Brun et al., 2010; Ercan-Sencicek et al., 2010; Haavik et al., 2008). PLP-dependent enzymes can be autoantigens and targets of the immune system in autoimmune disorders, *e.g.* Glu decarboxylase 65 (GAD65; GAD2) in type 1 diabetes (Baekkeskov et al., 1990), GAD67 (GAD1) and GAD65 in several neurological disorders (Graus et al., 2020), and cysteine sulphinic acid decarboxylase (CSAD) in autoimmune polyendocrine syndrome 1 (Sköldberg et al., 2004).

The sulphur-containing amino acid taurine is the most abundant free amino acid in mammals (Lourenco and Camilo, 2002; Samuelsson et al., 2012, 2013). Taurine is implicated in numerous physiological functions and attracts increasing attention as a biomarker for different disease states (Lourenco and Camilo, 2002; Samuelsson et al., 2012, 2013). It has a regulatory role in the maintenance of osmotic pressure and structural integrity of biological membranes (Hoffmann and Pedersen, 2006; Schaffer et al., 2010). In the nervous system, taurine may serve as a growth factor (Hernandez-Benitez et al., 2010; Pasantes-Morales and Hernández-Benítez, 2010) or a neurotransmitter/neuromodulator (Jia et al., 2008; Lähdesmäki et al., 1977). In many species, taurine deficiency can be lethal or associated with severe disease (Hoffmann and Pedersen, 2006), and in humans, altered levels of taurine have been reported in *e.g.* attention deficit hyperactivity disorder and autism (Hobert et al., 2014). In addition, taurine levels significantly decrease after electroconvulsive treatment in depressed patients, and this decrease strongly correlated with clinical improvements (Samuelsson et al., 2012, 2013). Plasma taurine levels were reduced by 83% in CSAD-deficient mice, and most offspring from 2nd-generation *Csad*$^{-/-}$ mice died shortly after birth, unless given taurine supplementation (Park et al., 2014), indicating a crucial physiological role for CSAD in taurine biosynthesis.

In mammalian tissues, taurine is mainly synthesised from cysteine in a three-step pathway, involving oxidation by cysteine dioxidase (E.C. 1.13.11.20), decarboxylation of cysteine sulphinic acid (CSA) by CSAD (E.C. 4.1.1.29), and oxidation of hypotaurine to taurine. CSA can additionally be decarboxylated by the related enzyme glutamic acid decarboxylase-like protein 1 (GADL1) (Winge et al., 2015), and taurine can be formed from cysteamine by cysteamine dioxygenase (E.C. 1.13.11.19) (Stipanuk et al., 2009).

Both CSAD and GADL1 are PLP-dependent decarboxylases (PLP-DC). GADL1, being the closest homologue, displays similar activity as CSAD (Winge et al., 2015). GADL1 plays a role in the decarboxylation of Asp to β-alanine and, thus, functions in the biosynthesis of the abundant dipeptides anserine and carnosine (Mahootchi et al., 2020). CSAD and GADL1 have distinct expression patterns in mouse and human brain (Winge et al., 2015). In the brain, CSAD has been detected in neurons and astrocytes in the cerebellum and hippocampus (Reymond et al., 1996; Chan-Palay et al., 1982). GADL1 is expressed in muscle, kidney, olfactory bulb, and isolated neurons (Winge et al., 2015; Liu et al., 2012). CSA is the preferred substrate for both CSAD and GADL1, although both are able to decarboxylate cysteic acid (CA) and Asp (Winge et al., 2015).

In an attempt to understand the molecular mechanisms underlying the catalysis and regulation of GADL1 and CSAD, and to enable future development of optimised inhibitors, we previously solved the crystal structure of mouse GADL1 (Raasakka et al., 2018). Here, we determined the crystal structure of mouse CSAD (*Mm*CSAD) in the presence and absence of PLP. Comparisons of the active sites of PLP-DCs highlight substrate recognition determinants within the structurally conserved enzyme family. The structure of CSAD helps to understand the details in the biosynthesis of taurine, one of the most abundant amino acids and dietary supplements.

2. Results and discussion

Taurine, the most abundant free intracellular amino acid in humans, has been implicated in a range of different physiological functions, and it is valuable as an industrial product and dietary supplement. PLP-dependent decarboxylation of CSA was observed in liver extracts from several mammalian species in the 1950s (Sörbo and Heyman, 1957; Chatagner et al., 1958), and since then, the properties of CSAD and related PLP-dependent enzymes have been extensively studied. Our aim was to better understand biosynthesis of taurine and the substrate specificity of PLP-DCs, by way of structural characterisation of CSAD, which catalyses the conversion of CSA into hypotaurine (Fig. 1A).

2.1. The crystal structure of MmCSAD

A structure of human CSAD has been available at the PDB (entry 2JIS). However, no detailed information, comparative studies with related enzymes, or mechanistic investigations of CSAD are available. We solved the crystal structure of *Mm*CSAD, in order to provide a tool for further studies on CSAD catalysis and facilitate the design of small molecules that could be used to modify taurine-related metabolic pathways.

The crystal structure of *Mm*CSAD was solved at 2.1-Å resolution using synchrotron radiation (Table 1, Fig. 1B,C). The active site is fully occupied with PLP covalently attached to Lys305 as an internal aldimine, indicating that the structure corresponds to the catalytically competent form of *Mm*CSAD.

The electrostatic potential surface of CSAD (Fig. 1D) shows a high positive charge in the active-site cavity, and it is conceivable that this property is important in attracting negatively charged substrates. CSAD and GADL1 prefer amino acids with short acidic side chains as substrates, *i.e.* Asp, CA, and CSA, of which CSA is most favoured for both enzymes (Winge et al., 2015). On the other hand, Glu, homocysteic acid, and homocysteine sulphinic acid have been reported not to be substrates of CSAD (Winge et al., 2015; Do and Tappaz, 1996).

*Mm*CSAD presents the conserved fold of PLP-DCs, with the closest structural homologues in the PDB being human CSAD and mouse GADL1 (Table 2). A sequence alignment of selected homologues with known structure is shown in Fig. 2. High structural similarity was expected, since the chemical reaction catalysed by PLP-DCs is essentially identical, and the substrates differ from each other only by their respective side chain moieties. It is possible, however, that substrate side chain recognition in different PLP-DCs may cause small changes in the positioning of the reactive groups, thereby leading to different kinetic properties.

In addition to the catalytically crucial residue Lys305, which in all PLP-DCs forms the internal aldimine with PLP, other residues in the active site are relevant for substrate binding and catalysis (Fig. 3A). The residues interacting with PLP are highly conserved and include His191, which is stacked above the PLP aromatic ring. His191 is fully conserved in the PLP-DC family, and in addition to fixing PLP in a reactive conformation, its roles have been suggested to be central in coordinating the carboxyl group that will be released as CO_2 (Komori et al., 2012), as well as in protonating the quinonoid intermediate resulting from decarboxylation (Liang et al., 2019, 2017).

An additional crystal structure was solved and turned out to be the apo form of CSAD, with no electron density for PLP in the active site (Supplementary Fig. 1). Hence, this structure represents an inactive form of CSAD. The main difference between the apo and holo forms is the rotation of the His191 side chain to a conformation not compatible with the presence of PLP (Fig. 3B). Overall, the active site of CSAD is less ordered in the absence of PLP; thus, PLP binding will stabilise a catalytically competent conformation of the cavity. No larger-scale conformational changes were observed between the apo and holo enzymes, which is different from DDC, in which the structure of the apo form presented an open conformation, suggested to be linked to the mechanism of cofactor loading (Giardina et al., 2011). Interestingly, both

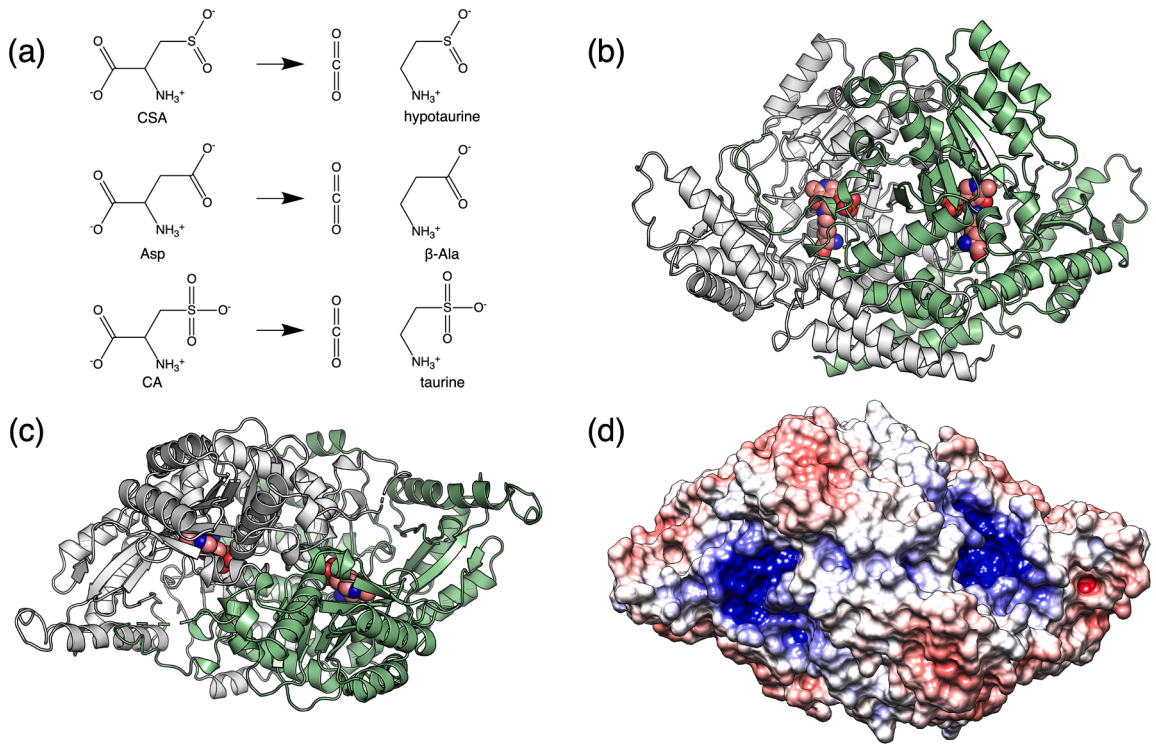

Fig. 1. Overall structure of *Mm*CSAD. (a) Reactions catalysed by CSAD. CSA is the preferred substrate. (b) Side view of the dimer. The active site is indicated by the internal aldimine between PLP and Lys305 (spheres). (c) Top view of the CSAD dimer. (d) Electrostatic surface shows positive potential (blue) in the active-site cavity (top view). (For interpretation of the references to colour in this figure legend, the reader is referred to the web version of this article.)

Table 1
Crystallographic data collection and refinement. Values in parentheses correspond to the highest-resolution shell.

Structure	CSAD holo	CSAD apo
Space group	$P2_1$	$P2_1$
Unit cell dimensions	a = 72.9, b = 113.3, c = 113.4 Å = γ = 90°, β = 95.8°	a = 73.1, b = 114.9, c = 113.8 Å = γ = 90°, β = 95.8°
Data processing		
Resolution range (Å)	50–2.10 (2.15–2.10)	50–2.80 (2.87–2.80)
Completeness (%)	90.7 (88.5)	98.6 (98.6)
R_{sym} (%)	12.5 (116.5)	42.6 (323.1)
R_{meas} (%)	15.1 (141.1)	50.4 (380.9)
$\langle I/\sigma(I)\rangle$	7.7 (0.9)	3.4 (0.4)
$CC_{1/2}$ (%)	99.3 (38.9)	94.9 (18.4)
Redundancy	2.7 (2.7)	3.4 (3.5)
Wilson *B* factor (Å^2)	39.2	55.1
Structure refinement		
R_{cryst}/R_{free} (%)	17.9/23.5	24.3/29.2
RMSD bond length (Å)	0.007	0.003
RMSD bond angle (°)	0.9	0.6
Ramachandran favoured/outliers (%)	96.3/0.16	95.6/0.16
MolProbity score/ percentile	1.61/96th	1.49/100th
PDB entry	6ZEK	7A0A

Table 2
Comparison of the mouse CSAD structure to selected PLP-DCs with known structure. Note how decrease in sequence identity has only minor effects on the similarity of the 3-dimensional fold.

Protein	PDB entry	Cα RMSD (Å)	Sequence identity (%)	Reference
human CSAD	2JIS	0.5	90	–
mouse GADL1	6ENZ	1.0	62	(Raasakka et al., 2018)
human GAD65	2OKK	0.8	54	(Fenalti et al., 2007)
human GAD67	2OKJ	1.0	53	(Fenalti et al., 2007)
human HDC	4E1O	2.1	21	(Komori et al., 2012)
pig DDC	1JS6	2.2	22	(Burkhard et al., 2001)
Arabidopsis thaliana phenylacetaldehyde synthase	6EEI	2.1	13	(Torrens-Spence et al., 2020)

CSAD structures were obtained from the same protein batch, indicating that PLP has been lost during crystallisation of the apo form. One possibility is hydrolysis of the internal aldimine at the slightly acidic pH (6.5) of the conditions giving the apo CSAD crystals, eventually leading to loss of PLP from the active site.

2.2. Structure of CSAD in solution

In addition to the crystal structure, we studied CSAD conformation in solution using synchrotron small-angle X-ray scattering (SAXS) (Fig. 4), in order to detect possible flexibility, as previously observed for GADL1 (Raasakka et al., 2018). Indeed, dimeric CSAD behaves much like GADL1 in solution, providing evidence for motions between open and closed states of the dimer. Such motions might be related to the catalytic cycle. They could be linked to the conformation of the flexible catalytic loop (residues 330–340), which is not fully visible in the CSAD crystal structure. Like in GADL1 (Raasakka et al., 2018), normal mode analysis identified an open conformation of the CSAD homodimer, which fits the SAXS data well (Fig. 4), but is different from that observed crystallographically for apo-DDC (Giardina et al., 2011). Whether open/close motions are unique to each class of PLP-DCs, or if all family members are equally dynamic, remains a subject for future research.

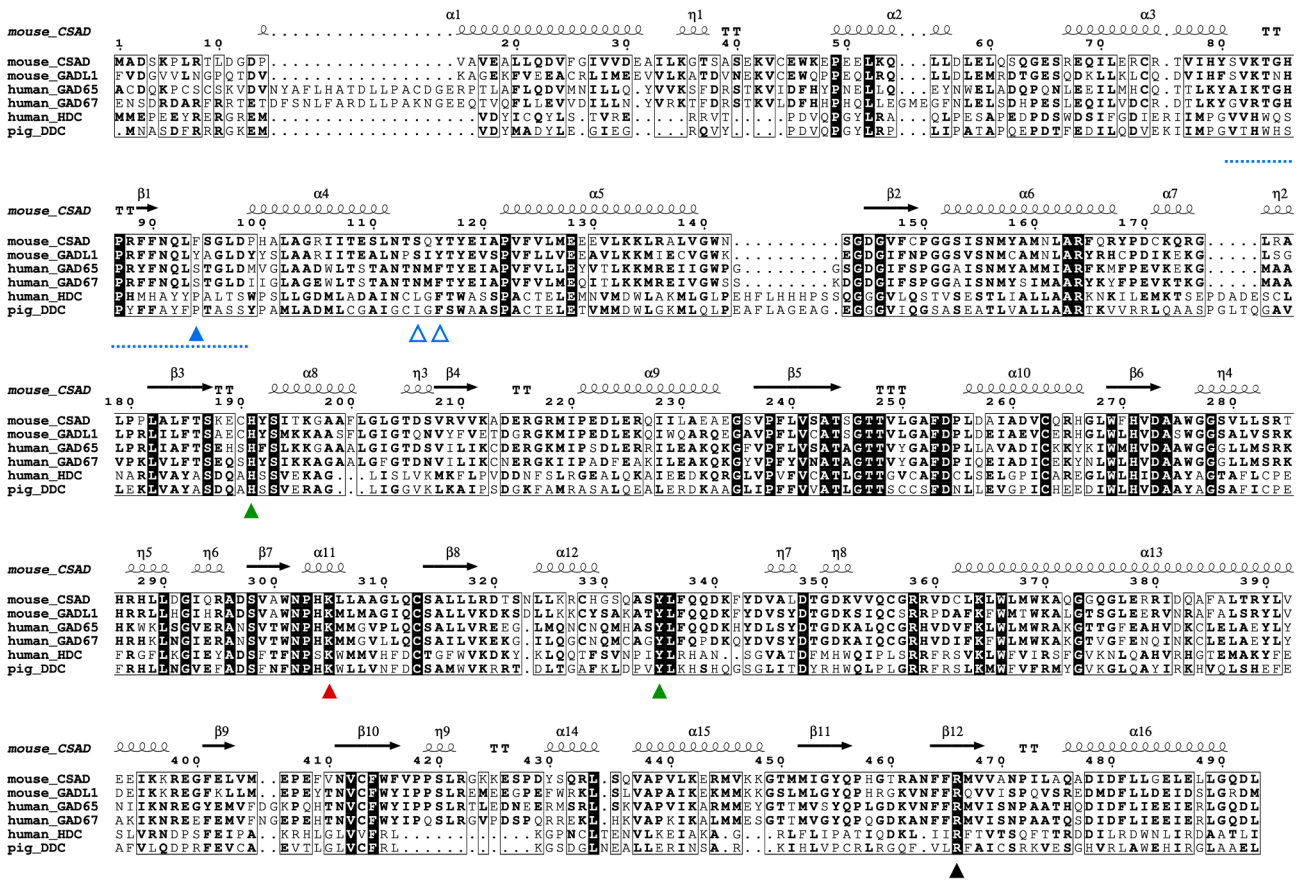

Fig. 2. Sequence alignment of PLP-DCs with known structure. Key elements discussed in the text are highlighted: Phe94 (blue), Ser114/Tyr116 (blue open), α3-α4 loop (blue dash), His191 (green), Lys305 (red), Tyr335 (green), Arg466 (black). Residue numbering corresponds to *Mm*CSAD. (For interpretation of the references to colour in this figure legend, the reader is referred to the web version of this article.)

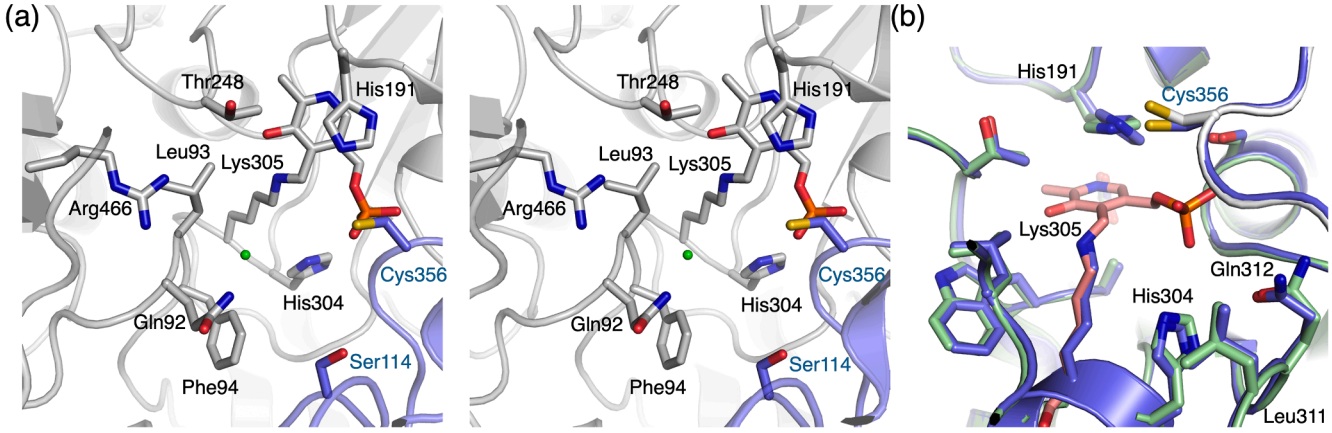

Fig. 3. The active site of *Mm*CSAD. (a) Stereo view of the CSAD active site. The bound chloride ion is shown as a green sphere. Elements coming into the active site from the opposing monomer are in blue. (b) Comparison of the holo (green/pink) and apo (blue) CSAD active sites. (For interpretation of the references to colour in this figure legend, the reader is referred to the web version of this article.)

2.3. Importance of Phe94 for substrate specificity

When comparing the structures of CSAD and GAD, it can be concluded that Phe94 in CSAD may be important for substrate specificity. Apparently, Phe94 blocks the binding site for larger substrates; hence, Glu should not productively bind (Fig. 5A). The active site of GAD has a Ser residue at the corresponding position. In addition, GADL1 has a Tyr residue at this position, linked to a slightly different substrate preference (Winge et al., 2015). We previously identified this position as a key difference in the substrate recognition pocket in the otherwise highly homologous acidic amino acid decarboxylases (Mahootchi et al., 2020). Thus, we mutated Phe94 to Ser in CSAD to evaluate the effects on enzymatic properties.

Activity assays of wild-type (WT) and F94S *Mm*CSAD towards CSA and Asp were carried out using HPLC (Table 3, Fig. 5B). While the F94S mutation affected both K_m and k_{cat} of CSAD towards CSA and Asp, the mutant enzyme remained active. Specifically, the effects on K_m and k_{cat} revealed that F94S has a turnover number 5–10 times lower than WT

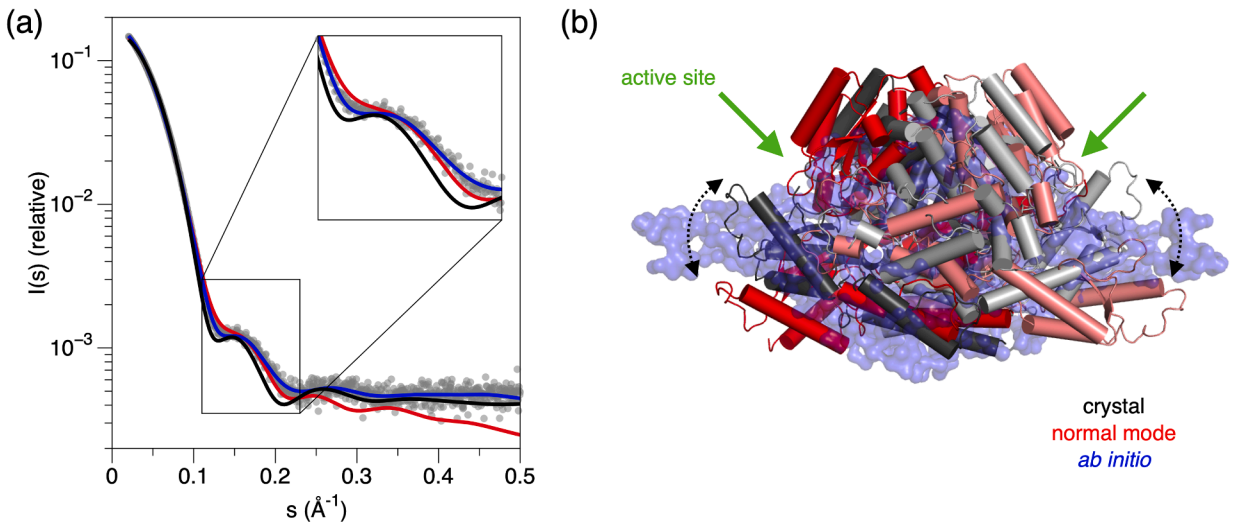

Fig. 4. Structure of *Mm*CSAD in solution. (a) SAXS data (grey dots) overlaid with fits from the crystal structure (black), the *ab initio* model (red), and the normal mode-based conformation (blue). (b) Comparison of the crystal structure and models. The open/close motions and the active site location are indicated. (For interpretation of the references to colour in this figure legend, the reader is referred to the web version of this article.)

CSAD for both CSA and Asp, indicating an overall effect on catalysis. In the mutant, K_m increases by an order of magnitude for CSA, but not for Asp. Hence, Phe94 is specifically important for the binding of CSA, the preferred substrate of CSAD. k_{cat}/K_m values further support these observations, showing that the most effective combination by far is WT CSAD with CSA as substrate.

A test for GAD activity was carried out using Glu as substrate, as the mutation F94S mimics the GAD substrate binding site (Fig. 5C). While a trace level of activity is observed for WT CSAD, this activity is even weaker for F94S. The K_m values for both variants are an order of magnitude higher than for CSA and Asp. Hence, altering the substrate specificity towards Glu requires more than altering the obvious Phe94 to the corresponding Ser residue of GAD. Additional factors may include protein dynamics, effects of the catalytic loop – not visible in any structure of CSAD or GADL1 – as well as minor conformational changes in the active site caused by the mutation.

2.4. Folding and stability of WT MmCSAD and F94S

The folding and thermal stability of WT *Mm*CSAD and F94S were examined using differential scanning fluorimetry (DSF) and circular dichroism (CD) spectroscopy. WT *Mm*CSAD and F94S show CD spectra with two characteristic minima at 208 and 220 nm. Both spectra are essentially identical, indicating correct folding of the mutant (Fig. 5D). Both CD spectroscopy and DSF indicate decreased thermal stability for the F94S mutant (Table 4). From the CD melting curves, it follows that although WT *Mm*CSAD and F94S have similar patterns of melting, F94S has a melting temperature ~ 5 °C lower than the WT protein (Fig. 5E). While the DSF melting curves indicate a similar decrease in stability for F94S (Fig. 5F), the mutant appears to open up already at low temperatures. The differences in T_m between the methods, which are commonly seen, could be because of differences in the measurement method between CD and DSF. While CD measures the unfolding of secondary structures based on peptide backbone conformation, DSF follows access of a small-molecule dye to the protein hydrophobic core.

The effect of the F94S mutation on the oligomeric state and long-term stability of *Mm*CSAD was further studied using size-exclusion chromatography (SEC) - multi-angle static light scattering (MALS), after freezing and thawing of a pure dimer fraction (Fig. 5G,H). Both WT *Mm*CSAD and F94S displayed very similar elution profiles, which mainly correspond to a dimer (110 kDa). Both variants also have some tetramer and higher-order oligomers after freezing and thawing (Fig. 5H). Notably, no monomeric form was detected, indicating high-affinity dimerisation; as the active site is formed at the dimer interface, this is expected.

Taken together, the F94S mutation does not affect the secondary structure content of CSAD, but it has a clear effect on protein stability. As the mutant displays lower activity than the WT enzyme, at least part of the effect could be from altered protein dynamics. These data indicate an important role for Phe94 in CSAD substrate binding and activity.

2.5. Comparison of the mouse CSAD active site with other decarboxylases

As far as enzymatic activity is concerned, CSAD is known to prefer CSA as substrate, while having weak activity towards CA and Asp (Winge et al., 2015; Do and Tappaz, 1996). The closest homologue, GADL1, is more active towards Asp than CSAD, although it is most active with CSA as substrate. Based on earlier studies, neither of the enzymes accept Glu as substrate, and Glu fails to act as an inhibitor (Winge et al., 2015), indicating lack of binding to the active site. It is possible that close members of the PLP-DC enzyme family have at least partially overlapping activities. Based on the observation that mice lacking GADL1 have organ-specific reductions of β-alanine and taurine levels, we recently suggested that this enzyme might have multiple physiological substrates also *in vivo* (Mahootchi et al., 2020). On the other hand, although our results indicate Glu is a very weak substrate for CSAD and GADL1, this activity is unlikely to be of any physiological relevance.

Using the high-resolution crystal structures of both CSAD and GADL1, as well as other PLP-DCs (Table 2), one can carry out an inspection of the corresponding active-site geometries underlying substrate specificity. As all PLP-DCs catalyse the same chemical reaction, amino acid decarboxylation, differences in the active site are expected to affect substrate specificity and/or affinity, rather than reaction mechanism *per se*. Hence, catalytically crucial features are expected to be conserved in sequence and 3D structure. For example, His191 is mechanistically important in PLP-DCs, possibly being involved in the protonation of the quinonoid reaction intermediate (Liang et al., 2019). Comparison of the apo and holo CSAD structures indicates that the conformation of His191 is linked to the presence of the PLP cofactor; it can be envisaged that His191 is important for the catalytically competent orientation of PLP and *vice versa*.

A comparison of CSAD and GADL1 should give indications on the structural properties causing their differential preference towards Asp,

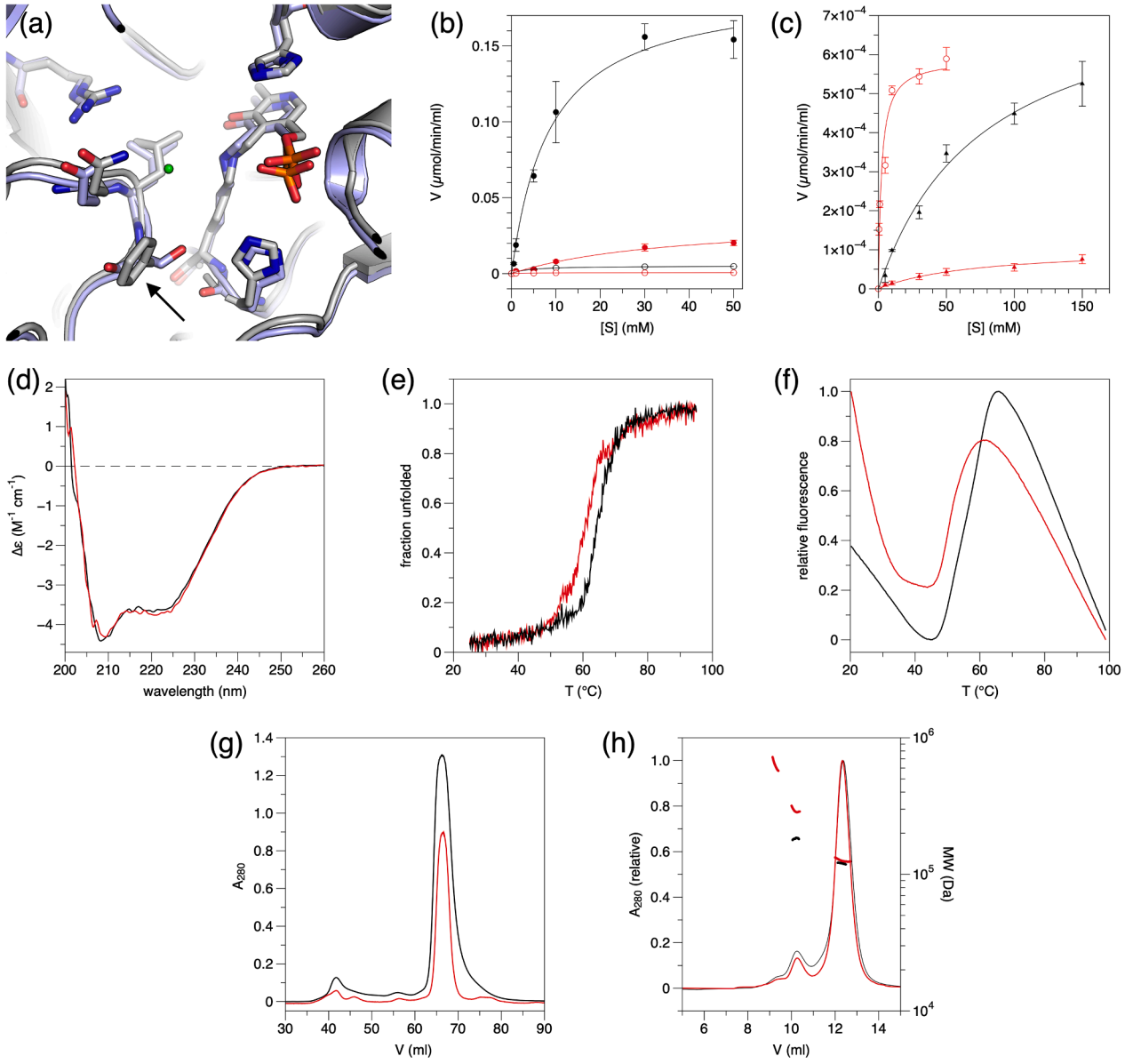

Fig. 5. Role of Phe94 in CSAD activity and stability. (a) Superposition of CSAD (grey) and GAD67 (light blue) active sites. The arrow indicates the position of CSAD Phe94. The chloride ion in CSAD is shown in green. (b) Activity assay with CSA (filled symbols) and Asp (open symbols). WT, black; mutant, red. (c) Activity assay with Glu (filled triangles). WT, black; mutant, red. The activity level of the mutant with Asp is shown for reference (red open circles). (d) CD spectra for WT (black) and mutant (red) CSAD. (e) CD melting curves. (f) DSF melting curves. (g) SEC during protein purification; the pure dimer peak at ~ 67 ml was picked for further experiments. (h) SEC-MALS after freezing and thawing of dimeric CSAD indicates presence of some higher-order oligomers in both WT and F94S. (For interpretation of the references to colour in this figure legend, the reader is referred to the web version of this article.)

Table 3
Enzymatic properties of CSAD towards acidic amino acids.

Substrate	WT CSAD k_{cat} (s^{-1})	K_m (mM)	k_{cat}/K_m (M^{-1} s^{-1})	F94S k_{cat} (s^{-1})	K_m (mM)	k_{cat}/K_m (M^{-1} s^{-1})
CSA	0.53 ± 0.02	8.6 ± 1.2	61.6	0.10 ± 0.01	36.8 ± 8.5	2.7
Asp	0.014 ± 0.004	3.8 ± 0.5	3.7	0.0016 ± 0.00006	2.3 ± 0.4	0.7
Glu	0.0022 ± 0.0002	77.3 ± 12.2	0.03	0.00029 ± 0.00004	72.6 ± 20.9	0.004

Table 4
Thermal stability of WT and F94S *Mm*CSAD.

Protein	DSF T_m (°C)	CD T_m (°C)
*Mm*CSAD	56.0 ± 0.2	64.6 ± 0.1
F94S	51.1 ± 0.2	60.5 ± 0.2

although CSA is the preferred substrate for both. Asp and CSA have slightly different geometries, in that the carboxyl group is planar while the sulphinic acid group is not. In addition, for the third known substrate, CA, the molecular size is larger, with 3 oxygen atoms interacting with the recognition pocket. In the predicted binding pocket for the acidic side-chain group, Phe94 in CSAD is replaced by Tyr in GADL1; while the hydroxyl group points away, minor changes in conformation and/or dynamics could explain the differences between CSAD and

GADL1. The Phe94 side chain and backbone of Gln92, Leu93, and Phe94 are likely to define the binding of the side chain in CSAD substrates (Fig. 5A).

When comparing CSAD and GAD65/67, it becomes obvious that Phe94 in CSAD is important for substrate specificity. It blocks the binding site for larger substrates, and the Ser residue at this position in GAD is likely to form hydrogen bonds to the Glu side chain carboxyl group (Fig. 6A). The binding mode of Glu into GAD can be deduced from the structure of GAD65 in complex with the inhibitor chelidonic acid (Fig. 6A) (Fenalti et al., 2007). Original studies on this line of inhibitors indicated that the distance between the two carboxyl groups, corresponding to an extended Glu molecule, is important (Porter and Martin, 1985). The carboxyl groups of the inhibitor mimic those of Glu, and hydrogen bonds are seen to Ser183/192 and a water molecule coordinated by His395/404 at the bottom of the cavity (numbering for GAD65/67), and well as to the backbone amide groups of the α3-α4 recognition loop containing Ser183/192 (see below). The His residue and the water molecule are also present in CSAD, and CSA is likely to

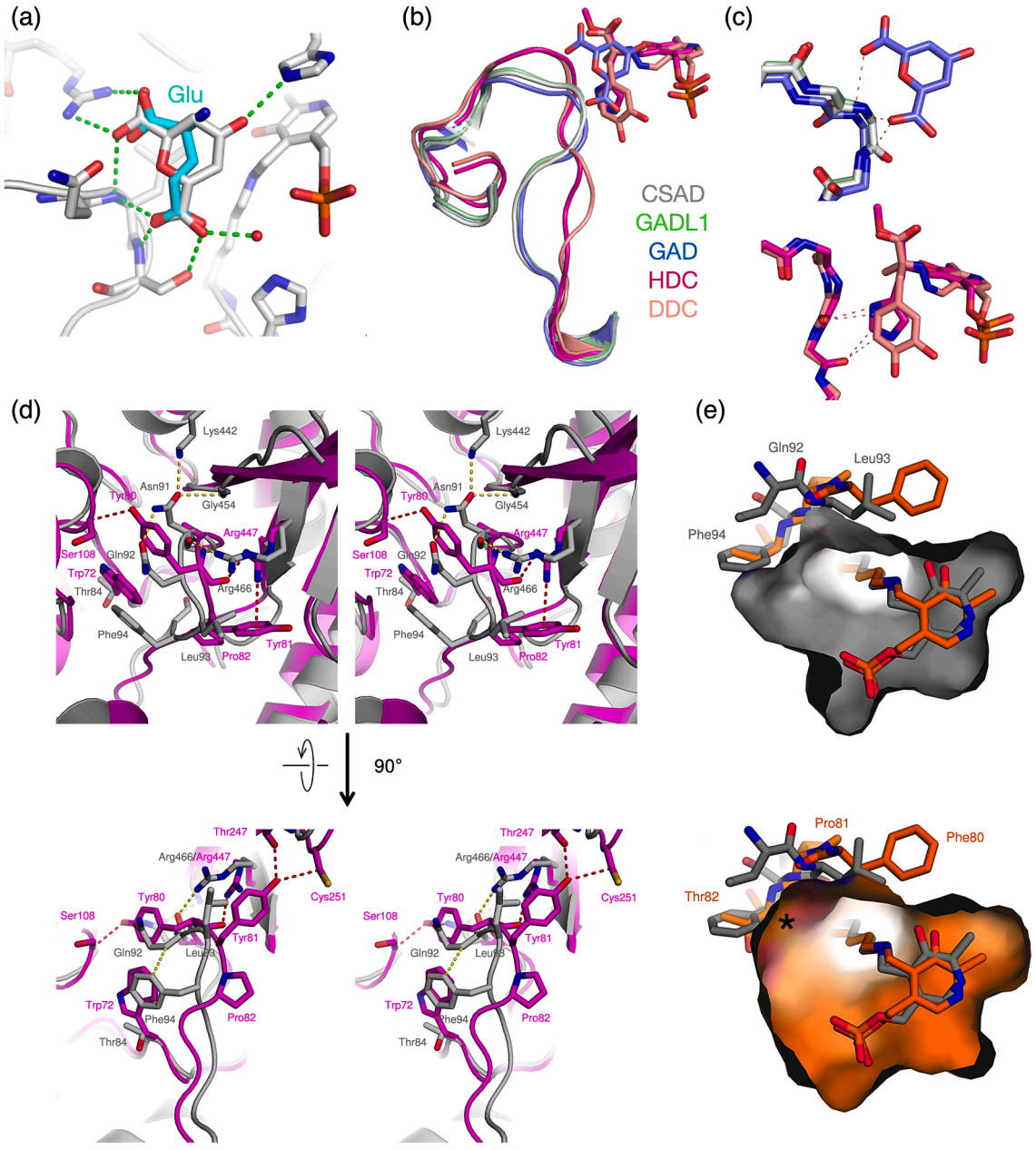

Fig. 6. Comparison to other decarboxylases. (a) GAD65 in complex with chelidonic acid, with hydrogen bonds shown in green. Based on the structure, a proposed mode of Glu substrate binding in GAD is shown (cyan). (b) Superposition of the α3-α4 loop in CSAD (grey), GADL1 (green), GAD65 (blue), HDC (magenta), and DDC (pink) highlights two subfamilies linked to substrate side chain size and properties. (c) Top: Backbone conformation in acidic amino acid decarboxylases (with chelidonic acid). Amino groups from the α3-α4 loop form direct hydrogen bonds (dashes) with the acidic substrate. Bottom: Backbone conformation in HDC and DDC; carbonyl groups interact with the substrate *via* hydrogen bonds and/or van der Waals interactions (dashes). (d) Stereo view of superposed CSAD (gray) and HDC (magenta) from two orientations. Key interactions of the α3-α4 loop of CSAD (yellow dashes) and HDC (red dashes) are shown. Additionally, large substituting changes between HDC and CSAD, such as Trp72/Thr84, are shown. (e) The α3-α4 loop and the internal aldimine in CSAD (grey) and DDC (orange). The surface at the top corresponds to CSAD and the one at the bottom to DDC. The black asterisk marks a volume present in DDC but not in CSAD, arising from the conformation of the α3-α4 loop. Relevant residues in the α3-α4 loop are labelled. (For interpretation of the references to colour in this figure legend, the reader is referred to the web version of this article.)

similarly hydrogen bond to this water molecule.

HDC has been crystallised with the non-cleavable His methyl ester trapped as a PLP adduct, thereby giving insights into the reaction mechanisms in the family (Komori et al., 2012). A similar conformation was observed for the inhibitor carbidopa in DDC (Burkhard et al., 2001). Phe94 in CSAD prevents the binding of such large substrates into the active site, but it is, in fact, not the only determinant. Comparing the acidic amino acid decarboxylases GAD65, GAD67, CSAD, and GADL1 with those acting on larger, non-acidic substrates, one should note the α3-α4 loop, forming the active site cavity wall and intimately interacting with the substrate (Fig. 6B). The backbone conformation of the α3-α4 loop is different between the two groups of enzymes, and the peptide bonds have opposite orientations, such that the NH groups point towards the substrate-binding cavity in GAD, CSAD, and GADL1 (Fig. 6C). In HDC and DDC, the carbonyl groups point into the same pocket, giving a different electrostatic environment and allowing the binding of positively charged and neutral substrates, such as His or L-DOPA, into the active site (Fig. 6C).

In addition to the active-site conformation, based on the sequence conservation of the α3-α4 recognition loop in PLP-DCs (Fig. 2), CSAD, GADL1, and the GADs can be grouped together, while DDC and HDC form another group (Fig. 6B). A closer comparison of mouse CSAD and human HDC reveals that the loop is formed out of two overlapping motifs forming central interactions close to the active site (Fig. 6D). In CSAD, the first motif stretches from Phe90 to Phe94, with the consensus sequence FNQ[FYS] in the first group. In HDC, the stretch that superimposes with this sequence involves Ala79-Pro82, with the consensus sequence AY[YF]P in the second group. The backbone trace of this segment in both groups is similar, although the underlying interactions and side chain conformations differ drastically between CSAD and HDC. In group 1, the central Asn residue acts as a hub of weak interactions and hydrogen bonds, locking different structural elements in place. For CSAD, a noteworthy Asn91-interacting residue is Lys442, which is fully conserved in the first group and likely to draw the α3-α4 loop towards helix α15. Worth noting is that Arg466 in CSAD (Arg447 in HDC) is fully conserved in PLP-DCs discussed above (Fig. 2), but may adopt different conformations. Its conservation is linked to its direct mechanistic interaction with the substrate α-carboxyl group.

Strikingly, the second stretch that follows after the conserved motif adopts a completely different conformation between the two groups of PLP-DCs (Fig. 6D). The conformation is influenced by the Pro residue replacing CSAD Phe94 in HDC and DDC, which leads to substantially more space in the active site of PLP-DCs with larger, non-acidic substrates (Fig. 6C,E). This is a key substrate binding determinant between the two groups of PLP-DCs. In addition to the conformational change resulting from the interaction network of the short sequence motifs, the rigidity of the α3-α4 loop is most likely different between the two groups. HDC and DDC have a conserved Trp residue (Trp72 in HDC), which is replaced by Thr84 in CSAD (Fig. 6D); hence, the α3-α4 loop in HDC and DDC may be more rigid. This is supported by lower *B* factors for the corresponding region (10 – 11 Å^2 in HDC bound to His methyl ester (resolution 1.8 Å), 21 – 25 Å^2 in apo-DDC (2.6 Å), 27 – 31 Å^2 in apo-CSAD (2.1 Å)).

2.6. Substrate specificity and catalytic mechanism of CSAD and GADL1

The substrate specificity of CSAD has been subject to some controversy. Before the availability of recombinant, purified enzyme, a concern was that the ability of CSAD to accept multiple substrates could be due to contamination with other enzymes, mainly GAD (Do and Tappaz, 1996; Guion-Rain and Chatagner, 1972; Oertel et al., 1981). However, we now know that CSA is the preferred substrate for CSAD both *in vitro* and *in vivo* (Park et al., 2014; Winge et al., 2015; Agnello et al., 2013). In addition, CSAD isolated from marine bacteria, insects, and several mammalian species accept CA, the oxidised form of CSA, as substrate, with 3–13% rate constants relative to CSA (Agnello et al., 2013; Liu et al., 2012). However, as the concentration of CA in the rat brain is 50–80% of CSA, decarboxylation of CA should have minor contribution to the overall synthesis of taurine (Ida and Kuriyama, 1983), at least in brain tissue. In addition, low Asp and Glu decarboxylase activity has been reported for CSAD (Winge et al., 2015; Weinstein and Griffith, 1987). Due to the presence of related enzymes with higher efficacy towards Asp and Glu (GADL1, GAD65, and GAD67), the physiological importance of such weak activity is unclear. However, the ability of the PLP-DCs to process a range of overlapping substrates may be metabolically advantageous, as observed for GADL1 knockout mice. These mice showed tissue-specific loss of both β-alanine and taurine derivatives, depending on the relative tissue abundance of the different enzymes (Mahootchi et al., 2020).

Insect aspartate decarboxylase (ADC), which has high homology and similar catalytic properties to CSAD, prefers CSA as substrate, but is also active towards Asp and CA (Liu et al., 2012). When ADC was incubated with CSA in the presence of each of the 20 proteinogenic amino acids, the preferred substrate was still CSA (Liu et al., 2013). Since insect ADC and human CSAD share ~ 50% sequence identity (Liu et al., 2019), one can expect similar properties for ADC and CSAD.

A number of ions were detected in the *Mm*CSAD structure; including an ion modelled as chloride in each active site (Fig. 3A,5A), interacting with the backbone amide groups of loop α3-α4 discussed above. This site could be relevant for recognizing the substrate acidic side chain. In the structure of HDC with methylhistidine (Komori et al., 2012) covalently linked to the PLP cofactor, the binding determinants for the carboxyl and amino groups are well defined, while the inhibitor chelidonic acid bound to GAD (Fenalti et al., 2007a, 2007b) provides additional information. Using these structures as templates, one can dock in CSA, taking into account the anion-binding site in the active cavity (Fig. 7). We consider the latter to be a likely location for the CSA sulphinic acid group binding - or in the case of Asp, the side-chain carboxyl group. While both CSA and Asp require two hydrogen bonding partners for the side chain, CA needs three – it is likely that two of the hydrogen bonds are provided by the backbone amide groups in the α3-α4 loop and the third one by the conserved water molecule.

The leaving carboxyl group, in a perpendicular position to the plane formed by the PLP ring and the Schiff base moiety, is stabilised by Arg466 (Fig. 7A). It may also be hydrogen-bonded to His191, a central residue in the PLP-DC mechanism, as seen in the structure of HDC (Komori et al., 2012). In apo CSAD, His191 is rotated, and it will reach its correct conformation upon PLP complex formation. Thus, the core active site of CSAD appears pre-organised for catalysis, but only in the presence of the cofactor internal aldimine.

A main obstacle in fully understanding the mechanistic details of CSAD and GADL1 catalysis is the flexible α12-α13 loop covering the active site; this loop is not visible in any of the available CSAD or GADL1 crystal structures, but a conserved Tyr residue in it has been suggested to be a key player in catalysis by PLP-DCs, including GAD (Fenalti et al., 2007). This Tyr, Tyr335 in CSAD, is conserved in CSAD and GADL1 (Fig. 2). Importantly, in both DDC and HDC, the loop is susceptible to proteolysis, but gets protected, when an active-site ligand is bound (Burkhard et al., 2001; Fleming et al., 2004; Ishii et al., 1998). Hence, the dynamics of the loop are linked to the decarboxylase reaction cycle and occupancy of the active site. After decarboxylation, protonation of the reaction intermediate is carried out by Tyr335, which enables the reaction to proceed towards product release and reconstitution of the internal aldimine in the CSAD active site. The protonation could either occur directly (Fenalti et al., 2007) or be mediated through a water molecule coordinated by Tyr335 (Fernandes et al., 2017). Intriguingly, PLP-DCs can catalyse a different reaction involving molecular oxygen, if this Tyr residue is mutated to a Phe (Bertoldi et al., 2002; Bisello et al., 2020). His191 also appears to be relevant for the protonation step (Liang et al., 2019, 2017; Fernandes et al., 2017), but in light of current data, its likely role is the coordination of Tyr335.

A tripartite substrate selectivity motif was identified in GAD and

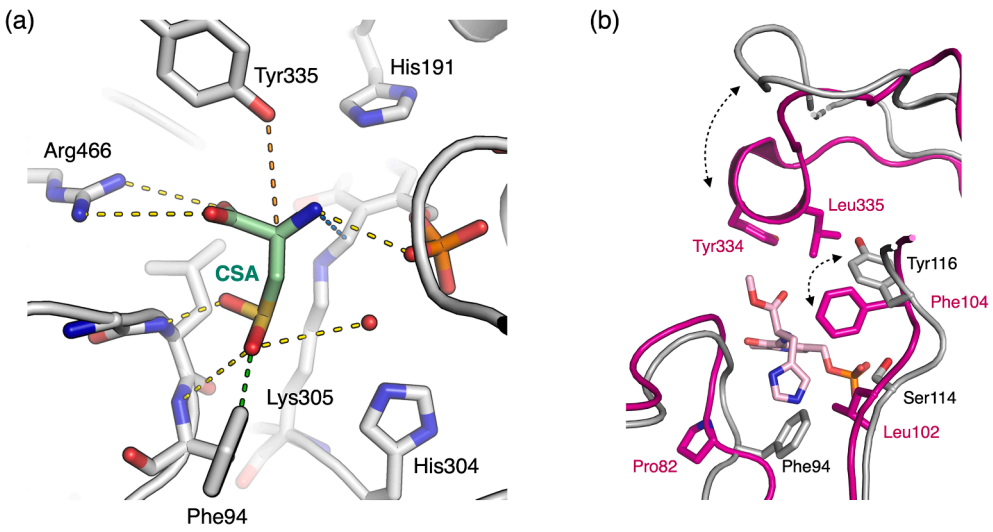

Fig. 7. Implications for the CSAD reaction mechanism. (a) Proposed model for CSA substrate binding to CSAD and depiction of catalytically important residues. Hydrogen bonds to active-site side chains, main-chain groups, the cofactor, and a conserved water molecule are shown in yellow dashes. A van der Waals interaction possibly relevant for CSAD substrate specificity to Phe94 is in green. The blue dash indicates the bond that will be formed upon external aldimine formation between Lys305 and CSA. Protonation of the quinonoid intermediate at the second stage of the reaction is likely catalysed by Tyr335 from the flexible α12-α13 catalytic loop (here pictured in the position observed in the GAD65 crystal structure), from the other subunit. (b) The previously identified CSAD/GAD substrate selectivity motif consisting of Phe94, Ser114, and Tyr116 (Agnello et al., 2013), compared to that in HDC (magenta). Note how the incoming loop containing the catalytic Tyr residue pushes the aromatic residue (Tyr116 in CSAD) in close contact with the catalytic cavity. (For interpretation of the references to colour in this figure legend, the reader is referred to the web version of this article.)

CSAD, in a study focusing on taurine synthesis by marine bacteria (Agnello et al., 2013). The residues of this motif are Phe94, Ser114, and Tyr116 in CSAD. Essentially, while Phe94 was important for catalysis on CSA and CA, replacing Tyr116 with Phe (as in GAD, DDC, or HDC), allowed CSAD to use Glu as substrate (Agnello et al., 2013). This brings an added level of complexity to the mechanism. Comparing the structure of CSAD with the enzymes carrying Phe at this position reveals a completely different conformation in the crystal state (Fig. 7B). In HDC and GAD, it is clear that the catalytic loop pushes the Phe residue to the active site wall, when the Tyr in this loop reaches in for protonation of the reaction intermediate. In the structures of CSAD and GADL1, the catalytic loop is disordered, and Tyr116 is in a relaxed conformation. During the reaction cycle, it must be pushed further in, reducing the available space in the active site, but also providing a putative additional hydrogen bonding contact for substrate recognition (Fig. 7B). The latter could be important in making CSA the preferred substrate for CSAD.

2.7. Insights into inhibitor design

Rare mutations in enzymes responsible for the degradation of β-alanine, as well as its histidine derivatives carnosine and anserine, have been linked to the abnormal accumulation of these compounds in mammalian tissues and severe neurological diseases (Scriver et al., 1966; Willi et al., 1997). As the neurological symptoms have been unresponsive to dietary interventions, an alternative treatment strategy could be to inhibit their biosynthesis. The discovery (Mahootchi et al., 2020) that GADL1 functions in the biosynthesis of β-alanine and carnosine raises the possibility that it could be a target for inhibition therapy. The first generation of inhibitors targeting CSAD and GADL1 had modest affinity but promising selectivity (Winge et al., 2015). Since then, high-resolution structures for both enzymes have become available, providing a stepping stone for further knowledge-based optimisation of such compounds. The differences in activity towards closely related substrates, as well as the subtle differences in the respective active-site structures, can be utilised in the development of a next generation of potential inhibitors of acidic amino acid decarboxylases. These aspects are crucial in the development of *in silico* screening approaches.

A prime example of inhibitor design towards PLP-DCs is carbidopa (Sletzinger et al., 1963), which is a DDC substrate analogue able to form a stable covalent adduct with the PLP cofactor. Carbidopa is in wide use in the treatment of Parkinson's disease, whereby it inhibits the conversion of L-DOPA to dopamine in peripheral tissues (Bartholini and Pletscher, 1975), leading to increased L-DOPA half-life and reduced side effects of dopamine. The crystal structure of DDC in complex with carbidopa (Burkhard et al., 2001) is, therefore, of high value in designing inhibitors towards other PLP-DCs. For example, for acidic amino acid decarboxylases, a similar approach targeting the external aldimine instead of a simple substrate analogue – as done previously (Winge et al., 2015; Porter and Martin, 1985; Liu et al., 2013) – would be a promising approach. In addition, mechanism-based inhibitors of CSAD activity, based on chemical substitutions on the β carbon, have been studied (Weinstein and Griffith, 1987; Griffith, 1983). Non-cleavable analogues of different stages of the acidic amino acid decarboxylase reaction mechanism could, hence, be targeted in a systematic manner instead of non-targeted screening or attempts at designing substrate analogues, which inherently will have rather low affinity in these enzymes.

3. Concluding remarks

Our work highlights central details of molecular mechanisms of taurine biosynthesis; in addition, substrate recognition determinants across the PLP-DC family have been elucidated. Substrate specificity in the family is clearly affected by both the amino acid side chains lining the catalytic cavity as well as direct backbone-substrate interactions. The latter divide PLP-DCs into two subclasses. These findings are central in understanding mechanistic details of catalysis, but also in research aimed at designing effectors of amino acid decarboxylation linked to the production of important metabolites and signalling molecules, such as taurine, β-alanine, carnosine, GABA, histamine, serotonin, and dopamine.

4. Materials and methods

4.1. Expression vector

Multiple mRNA transcripts of CSAD have been described, with alternative initiation codons and splicing events (Lourenco and Camilo,

2002). *Mm*CSAD cDNA corresponding to the 493-amino-acid (55 kDa; UniProt entry Q9DBE0) isoform was subcloned into the expression vector pTH27 (Hammarström et al., 2006), which codes for an N-terminal His_6 tag. In order to examine structural determinants of substrate specificity of *Mm*CSAD, the variant F94S was generated using the QuikChange kit (Agilent). The sequences of expression clones were verified by DNA sequencing.

4.2. Expression and purification of MmCSAD

WT and F94S His_6-CSAD were expressed in *Escherichia coli* BL21 CodonPlus (DE3)-RIPL cells (Stratagene) at +15 °C using 0.5 mM IPTG induction. Pyridoxine hydrochloride, a precursor of PLP biosynthesis, was added to the culture at 2 mM to improve protein solubility. Cell pellets were lysed by sonication in a buffer consisting of 50 mM sodium phosphate buffer pH 7.4, 500 mM NaCl, 20 mM imidazole, 0.2 mg/ml lysozyme, 1 mM $MgCl_2$, and cOmplete EDTA-free protease inhibitors (Roche). Phenylmethylsulphonyl fluoride was added to 1 mM immediately following sonication, and the unclarified lysate was applied onto an IMAC HiTrap TALON crude column (GE Healthcare). The column was washed first with 50 mM sodium phosphate pH 7.4, 500 mM NaCl, and then with the same buffer containing 20 mM imidazole. Elution was done with 100 mM imidazole in the same buffer. SEC was performed using a Superdex HR 200 column (GE Healthcare) equilibrated with 20 mM HEPES, 200 mM NaCl (pH 7.4). After elution, CSAD dimer fractions were combined and concentrated.

4.3. Crystallisation, data collection, structure solution, and refinement

*Mm*CSAD crystals were obtained at +20 °C using sitting-drop vapour diffusion. Holo-CSAD crystals were grown in drops containing 200 nl of protein stock (10.3 mg/ml) and 100 nl of reservoir solution (0.15 M KBr, 30% PEG2000 monomethyl ether), and apo-CSAD crystals grew in drops of 100 nl protein and 200 nl reservoir (200 mM Na_2SO_4, 100 mM Bis-tris propane, pH 6.5, 20% PEG3350). Crystals were briefly soaked in a cryoprotectant solution containing 80% reservoir solution and 20% glycerol, and flash-cooled in liquid N_2 prior to data collection.

X-ray diffraction data were collected at 100 K on the automated MASSIF-1 synchrotron beamline at ESRF (Grenoble, France) (Bowler et al., 2015; Bowler et al., 2016; Svensson et al., 2015). The data were processed and scaled using XDS (Kabsch, 2010). The structure was solved by molecular replacement in PHASER (McCoy et al., 2007), using the human CSAD crystal structure (PDB entry 2JIS) as template. Refinement was done in phenix.refine (Afonine et al., 2012) and model rebuilding with Coot (Casañal et al., 2020). The structures were validated using MolProbity (Chen et al., 2010).

4.4. Small-angle X-ray scattering

SAXS data for *Mm*CSAD were collected on the SWING beamline at the SOLEIL synchrotron (Gif-sur-Yvette, France). Scattering was measured in batch mode at three different protein concentrations (1–2.5 mg/ml), from a freshly purified monodisperse dimeric sample. The recorded frames were checked for radiation damage, and data from all concentrations were analysed to exclude interparticle effects. Data were processed using the beamline software Foxtrot 3.5.2 and analysed with ATSAS (Franke et al., 2017). *Ab initio* chain-like models were built with GASBOR (Svergun et al., 2001), normal mode-based conformations were analysed using SREFLEX (Panjkovich and Svergun, 2016), and the crystal structure was compared to the SAXS data with CRYSOL (Svergun et al., 1995).

4.5. Sequence and structure analysis

Structure superpositions were done with SSM (Krissinel and Henrick, 2004). Sequences were aligned with ClustalW (Thompson et al., 1994) and visualised with ESPript (Gouet et al., 1999). Electrostatic surfaces were calculated using APBS and pdb2pqr (Unni et al., 2011) and visualised in UCSF Chimera (Pettersen et al., 2004). PyMOL (Schrödinger) was used for structure visualisation and analysis.

4.6. Circular dichroism spectroscopy

CD spectra between 200 and 260 nm were recorded in triplicate on a Jasco J-810 instrument. Measurements were done at a protein concentration of 0.6 mg/ml in a 1-mm quartz cuvette. The samples were diluted with 10 mM sodium phosphate (pH 7.4), and buffer spectra were subtracted. Thermal denaturation was measured using the CD signal at 222 nm from +25 to +95 °C, at a heating rate of 2 °C/min.

4.7. Differential scanning fluorimetry

A fluorescence-based thermal stability assay (differential scanning fluorimetry, DSF) (Ericsson et al., 2006) was performed using a LightCycler 480 II instrument (Roche). 20-µl samples were analysed in 20 mM HEPES, 200 mM NaCl (pH 7.4). CSAD concentration was 0.1 mg/ml, and SYPRO® Orange was used at a 1:1000 (v/v) dilution. The instrument was set to detect emission between 300 and 570 nm. The heating rate was 2 °C/min from +20 to +99 °C. Five replicates of each sample were measured, using a 384-well plate with an optical film (Roche).

4.8. Quaternary structure analysis

Analytical SEC-MALS was employed to determine the oligomeric states of WT *Mm*CSAD and F94S. SEC was done using the ÄKTA™Purifier FPLC system (GE Healthcare), which was coupled with a RefractoMax 520 module (ERC GmbH, Riemerling, Germany) for measuring refractive index for concentration determination, and a miniDAWN TREOS light scattering detector (Wyatt Technology). Samples were diluted to 2 mg/ml and centrifuged at 16 000 *g* for 10 min at +4 °C. 200 µg of the protein were applied onto a Superdex 200 Increase 10/300 GL column, pre-equilibrated with 20 mM HEPES, 200 mM NaCl (pH 7.4), at a flow rate of 0.4 ml/min. Astra software (Wyatt) was used for SEC-MALS data analysis.

4.9. Enzymatic activity assays

Catalytic activity of WT *Mm*CSAD and F94S towards the known substrates CSA and Asp was measured at +37 °C, using a reaction mixture of 100 µl containing 6 µM CSAD, 60 mM potassium phosphate (pH 7.4), 5 mM DTT, and 0.5 µM PLP. Adding the amino acid substrate started the reaction. To measure steady-state kinetic properties of the enzymes, 0–50 mM of the substrates were tested. After 60 min, the reaction was stopped by addition of an equal volume of ice-cold ethanol containing 5% acetic acid. For studying GAD activity with Glu as substrate, the reaction mixture of 100 µl contained 60 mM potassium phosphate (pH 7.4), 5 mM DTT, and 2 mM PLP, and the reaction was stopped after 120 min.

The samples were centrifuged at 15,700 *g* for 10 min, and the supernatant was transferred onto a microtiter plate and analysed by HPLC. Samples were diluted with an equal volume of solvent (24% ethanol in 50 mM sodium phosphate, pH 6.0), and 4.2% *o*-phtaldialdehyde (OPA) reagent was added. Mobile phase was a mix of 50% of 100 mM sodium phosphate, 20% ethanol, and 30% H_2O. Flow rate was set to 0.5 ml/min. Samples were injected into a Zorbax Eclipse XDB-C18 column, and the product was determined based on fluorescence detection of the OPA-conjugated amino acid, using excitation at 366 nm and emission at 455 nm. Retention time for hypotaurine was 24.1 min, β-alanine 19.8 min, and GABA 31.1 min. The software used for detecting the area was ChemStation 1100 from Agilent. Kinetic parameters were determined by nonlinear regression using the Michaelis–Menten equation in GraphPad Prism 8 (GraphPad Software, La Jolla, California, USA).

5. Accession numbers

PDB: 6ZEK, 7A0A
SASBDB: SASDJR7

CRediT authorship contribution statement

Elaheh Mahootchi: Conceptualization, Formal analysis, Investigation, Methodology, Validation, Writing - original draft. **Arne Raasakka:** Conceptualization, Formal analysis, Investigation, Methodology, Validation, Writing - original draft. **Weisha Luan:** Investigation, Resources, Writing - review & editing. **Gopinath Muruganandam:** Investigation, Resources. **Remy Loris:** Resources, Supervision, Writing - review & editing. **Jan Haavik:** Conceptualization, Funding acquisition, Project administration, Supervision, Validation, Writing - review & editing. **Petri Kursula:** Conceptualization, Data curation, Formal analysis, Methodology, Project administration, Supervision, Validation, Visualization, Writing - original draft.

Declaration of Competing Interest

The authors declare that they have no known competing financial interests or personal relationships that could have appeared to influence the work reported in this paper.

Acknowledgements

This work has received funding from the European Union Horizon 2020 research and innovation program under Grant Agreement No. 810384 (CoCA), Stiftelsen Kristian Gerhard Jebsen (SKJ-MED-02), and the Regional Health Authority of Western Norway (No. 25048). This publication reflects only the authors' view, and the European Commission is not responsible for any use that may be made of the information it contains. We wish to acknowledge access to and excellent support on synchrotron beamlines at SOLEIL and ESRF.

Appendix A. Supplementary data

Supplementary data to this article can be found online at https://doi.org/10.1016/j.jsb.2020.107674.

References

Percudani, R., Peracchi, A., 2003. A genomic overview of pyridoxal-phosphate-dependent enzymes. EMBO Rep 4 (9), 850–854. https://doi.org/10.1038/sj.embor.embor914.

Thornton, J.M., Todd, A.E., Milburn, D., Borkakoti, N., Orengo, C.A., 2000. From structure to function: Approaches and limitations. Nat Struct Biol 7 (Suppl), 991–994. https://doi.org/10.1038/80784.

Liang, J., Han, Q., Tan, Y., Ding, H., Li, J., 2019. Current advances on structure-function relationships of pyridoxal 5'-phosphate-dependent enzymes. Front Mol Biosci 6, 4. https://doi.org/10.3389/fmolb.2019.00004.

Sarup, A., Larsson, O.M., Schousboe, A., 2003. GABA transporters and GABA-transaminase as drug targets. Curr Drug Targets CNS Neurol Disord 2, 269–277. https://doi.org/10.2174/1568007033482788.

Daidone F., Montioli R., Paiardini A., Cellini B., Macchiarulo A., Giardina G., et al. (2012). Identification by virtual screening and in vitro testing of human DOPA decarboxylase inhibitors. PLoS One 7, e31610.

Bartholini, G., Pletscher, A., 1975. Decarboxylase inhibitors. Pharmacology & Therapeutics. Part B: General and Systematic Pharmacology 1 (3), 407–421. https://doi.org/10.1016/0306-039X(75)90047-1.

Sletzinger, M., Chemerda, J.M., Bollinger, F.W., 1963. Potent decarboxylase inhibitors. Analogs of methyldopa. J Med Chem 6, 101–103. https://doi.org/10.1021/jm00338a003.

Brun, L., Ngu, L.H., Keng, W.T., Ch'ng, G.S., Choy, Y.S., Hwu, W.L., Lee, W.T., Willemsen, M.A.A.P., Verbeek, M.M., Wassenberg, T., Regal, L., Orcesi, S., Tonduti, D., Accorsi, P., Testard, H., Abdenur, J.E., Tay, S., Allen, G.F., Heales, S., Kern, I., Kato, M., Burlina, A., Manegold, C., Hoffmann, G.F., Blau, N., 2010. Clinical and biochemical features of aromatic L-amino acid decarboxylase deficiency. Neurology 75 (1), 64–71. https://doi.org/10.1212/WNL.0b013e3181e620ae.

Ercan-Sencicek, A.G., Stillman, A.A., Ghosh, A.K., Bilguvar, K., O'Roak, B.J., Mason, C.E., Abbott, T., Gupta, A., King, R.A., Pauls, D.L., Tischfield, J.A., Heiman, G.A., Singer, H.S., Gilbert, D.L., Hoekstra, P.J., Morgan, T.M., Loring, E., Yasuno, K., Fernandez, T., Sanders, S., Louvi, A., Cho, J.H., Mane, S., Colangelo, C.M., Biederer, T., Lifton, R.P., Gunel, M., State, M.W., 2010. L-Histidine Decarboxylase and Tourette's Syndrome. N Engl J Med 362 (20), 1901–1908. https://doi.org/10.1056/NEJMoa0907006.

Haavik, J., Blau, N., Thöny, B., 2008. Mutations in human monoamine-related neurotransmitter pathway genes. Hum. Mutat. 29 (7), 891–902. https://doi.org/10.1002/humu.20700.

Baekkeskov, S., Aanstoot, H.-J., Christgai, S., Reetz, A., Solimena, M., Cascalho, M., Folli, F., Richter-Olesen, H., Camilli, P.-D., 1990. Identification of the 64K autoantigen in insulin-dependent diabetes as the GABA-synthesizing enzyme glutamic acid decarboxylase. Nature 347 (6289), 151–156. https://doi.org/10.1038/347151a0.

Graus, F., Saiz, A., Dalmau, J., 2020. GAD antibodies in neurological disorders — insights and challenges. Nat Rev Neurol 16 (7), 353–365. https://doi.org/10.1038/s41582-020-0359-x.

Skoldberg F., Rorsman F., Perheentupa J., Landin-Olsson M., Husebye E. S., Gustafsson J., et al. (2004). Analysis of antibody reactivity against cysteine sulfinic acid decarboxylase, a pyridoxal phosphate-dependent enzyme, in endocrine autoimmune disease. J Clin Endocrinol Metab 89, 1636-1640.

Lourenco, R., Camilo, M.E., 2002. Taurine: A conditionally essential amino acid in humans? An overview in health and disease. Nutr Hosp 17, 262–270.

Samuelsson, M., Gerdin, G., Öllinger, K., Vrethem, M., 2012. Taurine and glutathione levels in plasma before and after ECT treatment. Psychiatry Research 198 (1), 53–57. https://doi.org/10.1016/j.psychres.2012.02.016.

Samuelsson, M., Skogh, E., Lundberg, K., Vrethem, M., Öllinger, K., 2013. Taurine and glutathione in plasma and cerebrospinal fluid in olanzapine treated patients with schizophrenia. Psychiatry Research 210 (3), 819–824. https://doi.org/10.1016/j.psychres.2013.09.014.

Hoffmann, E.K., Pedersen, S.F., 2006. Sensors and signal transduction pathways in vertebrate cell volume regulation. Contrib Nephrol 152, 54–104. https://doi.org/10.1159/000096318.

Schaffer, S.W., Ju Jong, C., KC, R., Azuma, J., 2010. Physiological roles of taurine in heart and muscle. J Biomed Sci 17 (Suppl 1), S2. https://doi.org/10.1186/1423-0127-17-S1-S2.

Hernandez-Benitez, R., Pasantes-Morales, H., Saldana, I.T., Ramos-Mandujano, G., 2010. Taurine stimulates proliferation of mice embryonic cultured neural progenitor cells. J Neurosci Res 88, 1673–1681. https://doi.org/10.1002/jnr.22328.

Pasantes-Morales, H., Hernández-Benítez, R., 2010. Taurine and Brain Development: Trophic or Cytoprotective Actions? Neurochem Res 35 (12), 1939–1943. https://doi.org/10.1007/s11064-010-0262-8.

Jia, F., Yue, M., Chandra, D., Keramidas, A., Goldstein, P.A., Homanics, G.E., Harrison, N. L., 2008. Taurine Is a Potent Activator of Extrasynaptic GABAA Receptors in the Thalamus. Journal of Neuroscience 28 (1), 106–115. https://doi.org/10.1523/JNEUROSCI.3996-07.2008.

Lähdesmäki, P., Kumpulainen, E., Raasakka, O., Kyrki, P., 1977. Interaction of taurine, GABA and glutamic acid with synaptic membranes. J Neurochem 29 (5), 819–826. https://doi.org/10.1111/j.1471-4159.1977.tb10724.x.

Hobert, J.A., Embacher, R., Mester, J.L., Frazier II, T.W., Eng, C., 2014. Biochemical screening and PTEN mutation analysis in individuals with autism spectrum disorders and macrocephaly. Eur J Hum Genet 22 (2), 273–276. https://doi.org/10.1038/ejhg.2013.114.

Park, E., Park, S.Y., Dobkin, C., Schuller-Levis, G., 2014. Development of a Novel Cysteine Sulfinic Acid Decarboxylase Knockout Mouse: Dietary Taurine Reduces Neonatal Mortality. Journal of Amino Acids 2014, 1–12. https://doi.org/10.1155/2014/346809.

Winge, I., Teigen, K., Fossbakk, A., Mahootchi, E., Kleppe, R., Sköldberg, F., Kämpe, O., Haavik, J., 2015. Mammalian CSAD and GADL1 have distinct biochemical properties and patterns of brain expression. Neurochemistry International 90, 173–184. https://doi.org/10.1016/j.neuint.2015.08.013.

Stipanuk, M.H., Ueki, I., Dominy Jr, J.E., Simmons, C.R., Hirschberger, L.L., 2009. Cysteine dioxygenase: a robust system for regulation of cellular cysteine levels. Amino Acids 37 (1). https://doi.org/10.1007/s00726-008-0202-y.

Mahootchi, E., Cannon, H.S., Kleppe, R., Winge, I., Hegvik, T.A., Megias-Perez, R., et al., 2020. GADL1 is a multifunctional decarboxylase with tissue-specific roles in beta-alanine and carnosine production. Sci Adv 6, eabb3713. https://doi.org/10.1126/sciadv.abb3713.

Reymond, I., Almarghini, K., Tappaz, M., 1996. Immunocytochemical localization of cysteine sulfinate decarboxylase in astrocytes in the cerebellum and hippocampus: a quantitative double immunofluorescence study with glial fibrillary acidic protein and S-100 protein. Neuroscience 75 (2), 619–633. https://doi.org/10.1016/0306-4522(96)00256-4.

Chan-Palay, V., Palay, S.L., Wu, J.-Y., 1982. Sagittal cerebellar microbands of taurine neurons: Immunocytochemical demonstration by using antibodies against the taurine-synthesizing enzyme cysteine sulfinic acid decarboxylase. Proceedings of the National Academy of Sciences 79 (13), 4221–4225. https://doi.org/10.1073/pnas.79.13.4221.

Liu, P., Ge, X., Ding, H., Jiang, H., Christensen, B.M., Li, J., 2012. Role of Glutamate Decarboxylase-like Protein 1 (GADL1) in Taurine Biosynthesis. J. Biol. Chem. 287 (49), 40898–40906. https://doi.org/10.1074/jbc.M112.393728.

Raasakka A., Mahootchi E., Winge I., Luan W., Kursula P. & Haavik J. (2018). Structure of the mouse acidic amino acid decarboxylase GADL1. Acta Crystallogr F Struct Biol Commun 74, 65-73.

Sörbo, B., Heyman, T., 1957. On the purification of cysteinesulfinic acid decarboxylase and its substrate specificity. Biochimica et Biophysica Acta 23, 624–627. https://doi.org/10.1016/0006-3002(57)90385-2.

Chatagner, F., Bergeret, B., Labouesse, J., 1958. Influence of thyroxin injection on the decarboxylation of L-glutamic acid by rat brain and of L-cysteine-sulfinic acid by rat liver. Biochim Biophys Acta 30, 422–423. https://doi.org/10.1016/0006-3002(58)90067-2.

Do, K.Q., Tappaz, M.L., 1996. Specificity of cysteine sulfinate decarboxylase (CSD) for sulfur-containing amino-acids. Neurochem Int 28, 363–371. https://doi.org/10.1016/0197-0186(95)00109-3.

Komori, H., Nitta, Y., Ueno, H., Higuchi, Y., 2012. Structural Study Reveals That Ser-354 Determines Substrate Specificity on Human Histidine Decarboxylase. J. Biol. Chem. 287 (34), 29175–29183. https://doi.org/10.1074/jbc.M112.381897.

Liang, J., Han, Q., Ding, H., Li, J., 2017. Biochemical identification of residues that discriminate between 3,4-dihydroxyphenylalanine decarboxylase and 3,4-dihydroxyphenylacetaldehyde synthase-mediated reactions. Insect Biochemistry and Molecular Biology 91, 34–43. https://doi.org/10.1016/j.ibmb.2017.10.001.

Giardina, G., Montioli, R., Gianni, S., Cellini, B., Paiardini, A., Voltattorni, C.B., Cutruzzola, F., 2011. Open conformation of human DOPA decarboxylase reveals the mechanism of PLP addition to Group II decarboxylases. Proceedings of the National Academy of Sciences 108 (51), 20514–20519. https://doi.org/10.1073/pnas.1111456108.

Fenalti, G., Hampe, C.S., O'Connor, K., Banga, J.P., Mackay, I.R., Rowley, M.J., El-Kabbani, O., 2007a. Molecular characterization of a disease associated conformational epitope on GAD65 recognised by a human monoclonal antibody b96.11. Molecular Immunology 44 (6), 1178–1189. https://doi.org/10.1016/j.molimm.2006.06.025.

Porter, T.G., Martin, D.L., 1985. Chelidonic acid and other conformationally restricted substrate analogues as inhibitors of rat brain glutamate decarboxylase. Biochemical Pharmacology 34 (23), 4145–4150. https://doi.org/10.1016/0006-2952(85)90207-2.

Burkhard, P., Dominici, P., Borri-Voltattorni, C., Jansonius, J.N., Malashkevich, V.N., 2001. Structural insight into parkinson's disease treatment from drug-inhibited DOPA decarboxylase. Nat Struct Biol 8, 963–967. https://doi.org/10.1038/nsb1101-963.

Guion-Rain, M.-C., Chatagner, F., 1972. Rat liver cysteine sulfinate decarboxylase: Some observations about substrate specificity. Biochimica et Biophysica Acta (BBA) - Enzymology 276 (1), 272–276. https://doi.org/10.1016/0005-2744(72)90029-0.

Oertel, W.H., Schmechel, D.E., Weise, V.K., Ransom, D.H., Tappaz, M.L., Krutzsch, H.C., et al., 1981. Comparison of cysteine sulphinic acid decarboxylase isoenzymes and glutamic acid decarboxylase in rat liver and brain. Neuroscience 6, 2701–2714. https://doi.org/10.1016/0306-4522(81)90114-7.

Agnello, G., Chang, L.L., Lamb, C.M., Georgiou, G., Stone, E.M., 2013. Discovery of a Substrate Selectivity Motif in Amino Acid Decarboxylases Unveils a Taurine Biosynthesis Pathway in Prokaryotes. ACS Chem. Biol. 8 (10), 2264–2271. https://doi.org/10.1021/cb400335k.

Liu, P., Ding, H., Christensen, B.M., Li, J., 2012. Cysteine sulfinic acid decarboxylase activity of Aedes aegypti aspartate 1-decarboxylase: The structural basis of its substrate selectivity. Insect Biochemistry and Molecular Biology 42 (6), 396–403. https://doi.org/10.1016/j.ibmb.2012.02.001.

Ida, S., Kuriyama, K., 1983. Simultaneous determination of cysteine sulfinic acid and cysteic acid in rat brain by high-performance liquid chromatography. Analytical Biochemistry 130 (1), 95–101. https://doi.org/10.1016/0003-2697(83)90654-1.

Weinstein, C.L., Griffith, O.W., 1987. Multiple forms of rat liver cysteinesulfinate decarboxylase. J Biol Chem 262, 7254–7263.

Liu, P., Torrens-Spence, M.P., Ding, H., Christensen, B.M., Li, J., 2013. Mechanism of cysteine-dependent inactivation of aspartate/glutamate/cysteine sulfinic acid alpha-decarboxylases. Amino Acids 44, 391–404. https://doi.org/10.1007/s00726-012-1342-7.

Liu, Z., Zheng, W., Ye, W., Wang, C., Gao, Y., Cui, W., et al., 2019. Characterization of cysteine sulfinic acid decarboxylase from Tribolium castaneum and its application in the production of beta-alanine. Appl Microbiol Biotechnol 103, 9443–9453. https://doi.org/10.1007/s00253-019-10139-z.

Fenalti, G., Law, R.H.P., Buckle, A.M., Langendorf, C., Tuck, K., Rosado, C.J., Faux, N.G., Mahmood, K., Hampe, C.S., Banga, J.P., Wilce, M., Schmidberger, J., Rossjohn, J., El-Kabbani, O., Pike, R.N., Smith, A.I., Mackay, I.R., Rowley, M.J., Whisstock, J.C., 2007b. GABA production by glutamic acid decarboxylase is regulated by a dynamic catalytic loop. Nat Struct Mol Biol 14 (4), 280–286. https://doi.org/10.1038/nsmb1228.

Fleming J. V., Sanchez-Jimenez F., Moya-Garcia A. A., Langlois M. R. & Wang T. C. (2004). Mapping of catalytically important residues in the rat l-histidine decarboxylase enzyme using bioinformatic and site-directed mutagenesis approaches. Biochem J 379, 253-261.

Ishii, S., Hayashi, H., Okamoto, A., Kagamiyama, H., 1998. Aromatic L-amino acid decarboxylase: Conformational change in the flexible region around arg334 is required during the transaldimination process. Protein Sci. 7 (8), 1802–1810. https://doi.org/10.1002/pro.5560070816.

Fernandes, H.S., Ramos, M.J., Cerqueira, N.M.F.S.A., 2017. The Catalytic Mechanism of the Pyridoxal-5′-phosphate-Dependent Enzyme, Histidine Decarboxylase: A Computational Study. Chem. Eur. J. 23 (38), 9162–9173. https://doi.org/10.1002/chem.201701375.

Bertoldi, M., Gonsalvi, M., Contestabile, R., Voltattorni, C.B., 2002. Mutation of Tyrosine 332 to Phenylalanine Converts Dopa Decarboxylase into a Decarboxylation-dependent Oxidative Deaminase. J. Biol. Chem. 277 (39), 36357–36362. https://doi.org/10.1074/jbc.M204867200.

Bisello, G., Longo, C., Rossignoli, G., Phillips, R.S., Bertoldi, M., 2020. Oxygen reactivity with pyridoxal 5′-phosphate enzymes: biochemical implications and functional relevance. Amino Acids 52 (8), 1089–1105. https://doi.org/10.1007/s00726-020-02885-6.

Scriver, C.R., Pueschel, S., Davies, E., 1966. Hyper-beta-alaninemia associated with beta-aminoaciduria and gamma-aminobutyricaciduaia, somnolence and seizures. N Engl J Med 274, 635–643. https://doi.org/10.1056/NEJM196603242741201.

Willi, S.M., Zhang, Y., Hill, J.B., Phelan, M.C., Michaelis, R.C., Holden, K.R., 1997. A deletion in the long arm of chromosome 18 in a child with serum carnosinase deficiency. Pediatr Res 41, 210–213. https://doi.org/10.1203/00006450-199702000-00009.

Griffith, O.W., 1983. Cysteinesulfinate metabolism. Altered partitioning between transamination and decarboxylation following administration of beta-methyleneaspartate. J Biol Chem 258, 1591–1598.

Hammarström, M., Woestenenk, E.A., Hellgren, N., Härd, T., Berglund, H., 2006. Effect of N-terminal solubility enhancing fusion proteins on yield of purified target protein. J Struct Funct Genomics 7 (1), 1–14. https://doi.org/10.1007/s10969-005-9003-7.

Bowler M. W., Nurizzo D., Barrett R., Beteva A., Bodin M., Caserotto H., et al. (2015). MASSIF-1: A beamline dedicated to the fully automatic characterization and data collection from crystals of biological macromolecules. Journal of synchrotron radiation 22, 1540-1547.

Bowler, M.W., Svensson, O., Nurizzo, D., 2016. Fully automatic macromolecular crystallography: the impact of MASSIF-1 on the optimum acquisition and quality of data. Crystallography Reviews 22 (4), 233–249. https://doi.org/10.1080/0889311X.2016.1155050.

Svensson O., Malbet-Monaco S., Popov A., Nurizzo D. & Bowler M. W. (2015). Fully automatic characterization and data collection from crystals of biological macromolecules. Acta Crystallographica Section D 71, 1757-1767.

Kabsch, W., 2010. XDS. Acta Crystallogr D Biol Crystallogr 66 (2), 125–132. https://doi.org/10.1107/S0907444909047337.

McCoy, A.J., Grosse-Kunstleve, R.W., Adams, P.D., Winn, M.D., Storoni, L.C., Read, R.J., 2007. Phaser crystallographic software. J Appl Crystallogr 40 (4), 658–674. https://doi.org/10.1107/S0021889807021206.

Afonine, P.V., Grosse-Kunstleve, R.W., Echols, N., Headd, J.J., Moriarty, N.W., Mustyakimov, M., Terwilliger, T.C., Urzhumtsev, A., Zwart, P.H., Adams, P.D., 2012. Towards automated crystallographic structure refinement with phenix.refine. Acta Crystallogr D Biol Crystallogr 68 (4), 352–367. https://doi.org/10.1107/S0907444912001308.

Casañal, A., Lohkamp, B., Emsley, P., 2020. Current developments in Coot for macromolecular model building of Electron Cryo-microscopy and Crystallographic Data. Protein Science 29 (4), 1055–1064. https://doi.org/10.1002/pro.3791.

Chen, V.B., Arendall III, W.B., Headd, J.J., Keedy, D.A., Immormino, R.M., Kapral, G.J., Murray, L.W., Richardson, J.S., Richardson, D.C., 2010. MolProbity : all-atom structure validation for macromolecular crystallography. Acta Crystallogr D Biol Crystallogr 66 (1), 12–21. https://doi.org/10.1107/S0907444909042073.

Franke D., Petoukhov M. V., Konarev P. V., Panjkovich A., Tuukkanen A., Mertens H. D. T., et al. (2017). Atsas 2.8: A comprehensive data analysis suite for small-angle scattering from macromolecular solutions. J Appl Crystallogr 50, 1212-1225.

Svergun, D.I., Petoukhov, M.V., Koch, M.H.J., 2001. Determination of Domain Structure of Proteins from X-Ray Solution Scattering. Biophysical Journal 80 (6), 2946–2953. https://doi.org/10.1016/S0006-3495(01)76260-1.

Panjkovich, A., Svergun, D.I., 2016. Deciphering conformational transitions of proteins by small angle X-ray scattering and normal mode analysis. Phys. Chem. Chem. Phys. 18 (8), 5707–5719. https://doi.org/10.1039/C5CP04540A.

Svergun, D., Barberato, C., Koch, M.H.J., 1995. CRYSOL – a Program to Evaluate X-ray Solution Scattering of Biological Macromolecules from Atomic Coordinates. J Appl Crystallogr 28 (6), 768–773. https://doi.org/10.1107/S0021889895007047.

Krissinel, E., Henrick, K., 2004. Secondary-structure matching (SSM), a new tool for fast protein structure alignment in three dimensions. Acta Crystallogr D Biol Crystallogr 60 (12), 2256–2268. https://doi.org/10.1107/S0907444904026460.

Thompson, J.D., Higgins, D.G., Gibson, T.J., 1994. CLUSTAL W: improving the sensitivity of progressive multiple sequence alignment through sequence weighting, position-specific gap penalties and weight matrix choice. Nucl Acids Res 22 (22), 4673–4680. https://doi.org/10.1093/nar/22.22.4673.

Gouet, P., Courcelle, E., Stuart, D., Metoz, F., 1999. ESPript: analysis of multiple sequence alignments in PostScript. Bioinformatics 15 (4), 305–308. https://doi.org/10.1093/bioinformatics/15.4.305.

Unni, S., Huang, Y., Hanson, R.M., Tobias, M., Krishnan, S., Li, W.W., Nielsen, J.E., Baker, N.A., 2011. Web servers and services for electrostatics calculations with APBS and PDB2PQR. J. Comput. Chem. 32 (7), 1488–1491. https://doi.org/10.1002/jcc.21720.

Pettersen, E.F., Goddard, T.D., Huang, C.C., Couch, G.S., Greenblatt, D.M., Meng, E.C., Ferrin, T.E., 2004. UCSF Chimera?A visualization system for exploratory research and analysis. J. Comput. Chem. 25 (13), 1605–1612. https://doi.org/10.1002/jcc.20084.

Ericsson, U.B., Hallberg, B.M., DeTitta, G.T., Dekker, N., Nordlund, P., 2006. Thermofluor-based high-throughput stability optimization of proteins for structural studies. Analytical Biochemistry 357 (2), 289–298. https://doi.org/10.1016/j.ab.2006.07.027.

Torrens-Spence, M.P., Chiang, Y.-C., Smith, T., Vicent, M.A., Wang, Y.i., Weng, J.-K., 2020. Structural basis for divergent and convergent evolution of catalytic machineries in plant aromatic amino acid decarboxylase proteins. Proc Natl Acad Sci USA 117 (20), 10806–10817. https://doi.org/10.1073/pnas.1920097117.